Journal of Power Sources 196 (2011) 8098–8103

Contents lists available at ScienceDirect

Journal of Power Sources

journal homepage: www.elsevier.com/locate/jpowsour

Nitroxide polymer brushes grafted onto silica nanoparticles as cathodes for organic radical batteries

Hsiao-Chien Lin [a], Chia-Chen Li [b], Jyh-Tsung Lee [a,*]

[a] Department of Chemistry and Center for Nano Science & Nano Technology, National Sun Yat-Sen University, Kaohsiung 80424, Taiwan
[b] Department of Materials and Mineral Resources Engineering, National Taipei University of Technology, Taipei 10608, Taiwan

ARTICLE INFO

Article history:
Received 15 February 2011
Received in revised form 11 April 2011
Accepted 16 May 2011
Available online 27 May 2011

Keywords:
Nitroxide polymer
Polymer brushes
Organic radical battery
Cathode
Nanoparticles
Atom transfer radical polymerization

ABSTRACT

Nitroxide polymer brushes grafted on silica nanoparticles as binder-free cathodes for organic radical batteries have been investigated. Scanning electron microscopy, transmission electron microscopy, infrared spectroscopy and electron spin resonance confirm that the nitroxide polymer brushes are successfully grafted onto silica nanoparticles *via* surface-initiated atom transfer radical polymerization. The thermogravimetric analysis results indicate that the onset decomposition temperature of these nitroxide polymer brushes is found to be ca. 201 °C. The grafting density of the nitroxide polymer brushes grafted on silica nanoparticles is 0.74–1.01 chains nm^{-2}. The results of the electrochemical quartz crystal microbalance indicate that the non-crosslinking nitroxide polymer brushes prevent the polymer from dissolving into organic electrolytes. Furthermore, the electrochemical results show that the discharge capacity of the polymer brushes is 84.9–111.1 mAh g^{-1} at 10 C and the cells with the nitroxide polymer brush electrodes have a very good cycle-life performance of 96.3% retention after 300 cycles.

1. Introduction

Recently, nitroxide radical polymers have attracted much attention because of their potential application to cathode-active materials for organic radical batteries [1–5]. Nitroxide radical polymers have several advantages, including being environmentally friendly and mechanically flexible [1]. Among nitroxide radical polymers, poly(2,2,6,6-tetramethylpiperidin-1-oxyl-4-yl methacrylate), PTMA, is one of the promising cathode-active materials for organic radical batteries. PTMA is a methacrylate backbone grafted with 2,2,6,6-tetramethylpiperidin-1-oxyl-4-yl, TEMPO. TEMPO is a very stable radical because the nitroxide radical ($NO^{\bullet}$) is protected by four methyl groups on the α-position and its stable resonance structures. The nitroxide radical is oxidized to an oxoammonium cation when charging, and the oxoammonium cation is reduced back to a nitroxide radical when discharging [2,3]. The energy capacity of PTMA is around 70–110 mAh g^{-1} [3–5]. PTMA has a high-rate charge and discharge performance because of its rapid electron-transfer process and high diffusion coefficient [4].

Unfortunately, nitroxide polymers may tend to dissolve into certain organic electrolytes when the polymer is solvophilic and non-crosslinking, which affects the energy density, self-discharge, and cycle-life performance of batteries [5]. Therefore, in order to inhibit the dissolution of polymers into electrolytes, several crosslinking methods have been reported [5–8].

Unlike a number of crosslinking methods, we have recently demonstrated a new non-crosslinking approach which grows PTMA brushes on indium tin oxide (ITO) substrates as thin-film cathodes for organic radical batteries *via* surface-initiated atom transfer radical polymerization (ATRP) to inhibit the dissolution of polymers into electrolytes [9]. The nitroxide polymer brushes were covalently bonded on silica nanoparticles, preventing the polymer from dissolving into electrolytes, which improves its electrochemical properties. However, the thin-film electrodes are plate-structural, which limits their energy and power capacities. Therefore, this paper reports the use of a non-crosslinking approach to grow nitroxide polymer brushes on silica nanoparticles for organic radical batteries to increase the energy capacity per area because of its higher grafting density. Most interestingly, the polymer brushes grafted onto silica nanoparticles can be processed by a slurry coating, and can serve as binder-free cathode-active materials to increase the energy density of organic radical batteries.

2. Experimental

2.1. Materials

2-Bromo-2-methylpropionyl bromide (98%), N,N,N′,N″,N″-pentamethyldiethylenetriamine (PMDETA, 99%), Karstedt's

* Corresponding author. Tel.: +886 7 525 3951; fax: +886 7 525 3951.
E-mail address: jtlee@faculty.nsysu.edu.tw (J.-T. Lee).

0378-7753/$ – see front matter © 2011 Elsevier B.V. All rights reserved.
doi:10.1016/j.jpowsour.2011.05.037

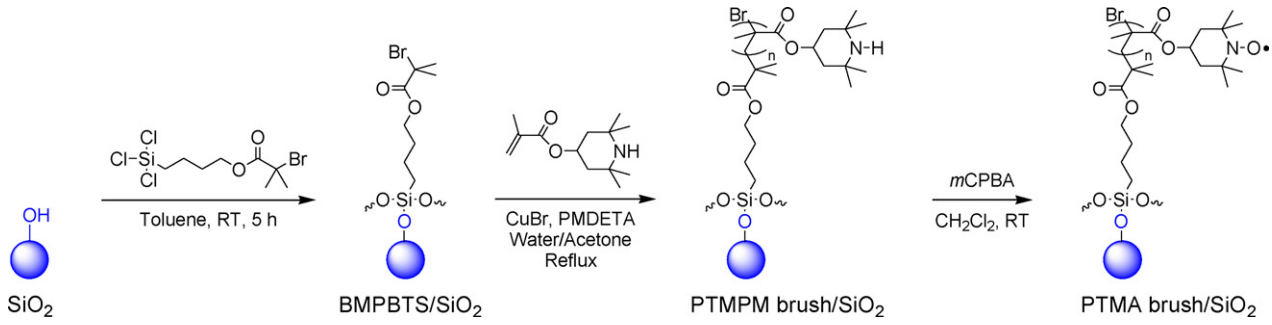

Scheme 1. Synthesis of PTMA brush on silica nanoparticles.

catalyst (~2% Pt), and copper (I) bromide (CuBr, 99.999%) were obtained from Aldrich. 3-Buten-1-ol (98%) and 2,2,6,6-tetramethyl-4-piperidyl methacrylate (TMPM, 98%) were purchased from TCI. Triethylamine (99%) and trichlorosilane (>98%) were obtained from J. T. Baker and SHOWA, respectively. *m*-Chloroperoxybenzoic acid (*m*CPBA, 70–75%, Acros) was recrystallized in methanol. 4-(Trichlorosilyl)butyl 2-bromo-2-methylpropanate (BMPBTS) was synthesized according to the previous published procedure [9]. The silica nanoparticles obtained from UniRigion Bio-Tech has particle sizes of about 15 and 40 nm. The silica nanoparticles with a particle size of 400 nm were synthesized by the Stöber method [10]. All the silica nanoparticles were calcined at 500 °C for 4 h in air.

2.2. Synthesis of PTMA on silica nanoparticles

The preparation of PTMA brushes grafted onto the silica nanoparticles is illustrated in Scheme 1. In order to attach the initiator on the silica nanoparticles, the silica nanoparticles (0.175 g) were immersed in a 10.0 mL of 0.03 M BMPBTS toluene solution at room temperature under an atmosphere of nitrogen for 5 h. Finally, the initiator-attached silica nanoparticles were washed with acetone three times, and then dried in a vacuum oven.

For ATRP, PMDETA (31.0 μL, 0.15 mmol) was dissolved in a 10.0 mL of the water/acetone (1/4 in volume) solution degassed by three freeze–pump–thaw cycles. This solution was transferred into a degassed flask containing CuBr (7.2 mg, 0.05 mmol), initiator-attached silica nanoparticles (0.134 g), and TMPM (1.127 g, 5.0 mmol). The surface-initiated ATRP was carried out at reflux under an atmosphere of nitrogen for 1 h to yield poly(2,2,6,6-tetramethylpiperidin-4-yl methacrylate) (PTMPM) brushes/silica nanoparticles. The PTMPM brushes/silica nanoparticles were washed and ultrasonicated with acetone three times, and then dried in a vacuum oven.

The PTMPM brushes/silica nanoparticles (0.013 g) were immersed in a 10.0 mL dichloromethane solution of *m*CPBA (0.017 g, 0.1 mmol) at room temperature for 10 min to yield PTMA brushes/silica nanoparticles which were then washed and ultrasonicated again with acetone three times and then dried in a vacuum oven.

2.3. Fabrication of PTMA brush/carbon composite electrode

The PTMA or PTMA brushes/silica nanoparticles (6 mg) and the conductive carbon (Super P, 18 mg) were dispersed in N-methyl-2-pyrrolidone (NMP, 0.5 mL) and stirred for 15 h. The above slurry was coated on aluminum foil (20 μm in thickness) by the doctor blade method and then the electrode was dried under a high vacuum at 60 °C for 15 h. The thickness of the composite layer was about 20 μm. The composite electrode consisted of 25 wt% PTMA or PTMA brushes/silica nanoparticles and 75 wt% Super P. The loading of the composite electrode was about 0.5 mg cm^{-2}.

2.4. Electrochemical measurements

For the electrochemical quartz crystal microbalance (EQCM) experiments, the electrochemical cell consisted of a quartz crystal gold electrode (with a 7.995-MHz fundamental frequency) as a working electrode, a platinum wire as a counter electrode, and a $Ag/AgNO_3$ (0.01 M $AgNO_3$ and 0.1 M tetra-*n*-butylammonium perchlorate, $(C_4H_9)_4NClO_4$, in acetonitrile) electrode as a reference electrode. The PTMA thin film or PTMA brush/silica nanoparticles were deposited on the gold working electrode; the electrolyte was 0.1 M $(C_4H_9)_4NClO_4$ in acetonitrile. The EQCM experiments were monitored between 0.3 and 0.6 V at a scan rate of 10 mV s^{-1}. In half-cell experiments, coin cells (CR2320) were assembled in an Ar-filled glove box using Celgard 2500 as a separator. A lithium foil was used as a counter electrode and a reference electrode. The PTMA brush composite electrode was used as a working electrode. The electrolyte was 1.0 M $LiClO_4$ in ethylene carbonate (EC)/diethyl carbonate (DEC) (=1:1 in volume). The cells were charged/discharged at a constant current at 10, 30, and 50 C between 3.0 and 4.0 V or cycled at 10 C between 3.0 and 4.0 V.

2.5. Instruments

The transmission Fourier transform infrared spectroscopy (FTIR) spectra were collected by a Perkin-Elmer spectrum 100 FTIR spectrometer, with a resolution of 4 cm^{-1}. Electron spin resonance (ESR) spectra were performed on a Bruker EMX-10 spectrometer. The morphology and shape of various samples were observed by means of a field emission scanning electron microscope (FESEM, JEOL JSM-6700F) using an accelerating voltage of 10 kV. The structures of various samples were obtained by a transmission electron microscope (TEM, PHILIPS CM-200 TWIN) with an accelerating voltage of 200 kV. The TEM specimens were typically prepared by ultrasonic dispersion of the PTMA brushes/silica nanoparticles in ethanol and then a drop of the supernatant was transferred onto a copper grid. Electrochemical properties were measured on a CHI model 405A electrochemical analytical instrument. The thermal stability of the resulting polymers was examined by means of a thermogravimetric analysis (TGA) with a TA Instruments model Q50 analyzer in an atmosphere of air at a heating rate of 10 °C min^{-1} from 40 to 800 °C. Electrochemical gel permeation chromatography (GPC) measurements were taken on a Shimadzu system in THF using a Waters' column at 45 °C, and the calibration was performed using a series of polystyrene standards.

3. Results and discussion

Fig. 1a–c shows the SEM micrographs for the bare silica nanoparticles with sizes of 15, 40, and 400 nm, respectively. The silica nanoparticles were further modified with the surface initiator, BMPBTS, of ATRP. The size and the surface morphology of the

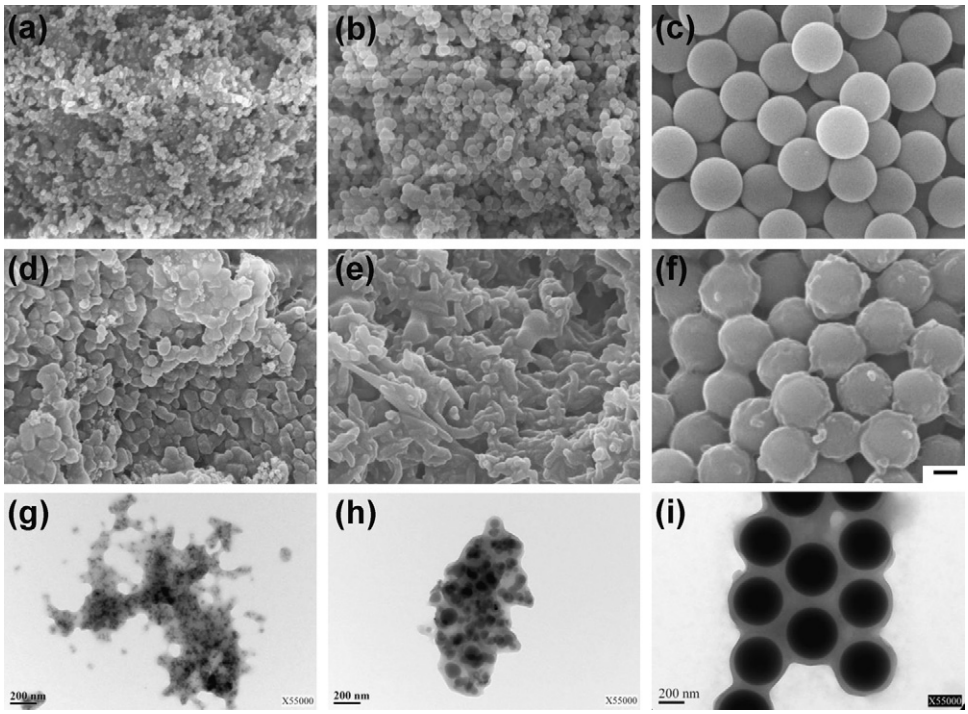

Fig. 1. SEM micrographs for the bare silica nanoparticles with a particle size of (a) 15 nm, (b) 40 nm, and (c) 400 nm, and the PTMA brush/silica nanoparticles with a particle size of (d) 15 nm, (e) 40 nm, and (f) 400 nm; the scale bar is 200 nm. TEM micrographs for the PTMA brush/silica nanoparticles with a particle size of (g) 15 nm, (h) 40 nm, and (i) 400 nm.

surface-initiator modified silica nanoparticles are similar to that of the bare silica nanoparticles. This is due to the fact that the thickness of the surface-initiator is very thin. After the surface-initiated ATRP of TMPM, PTMPM brushes were grafted onto the silica nanoparticles. Finally, the PTMPM brushes/silica nanoparticles were oxidized by *m*CPBA in dichloromethane to yield PTMA brushes/silica nanoparticles. The SEM micrograms in Fig. 1d–f show that the resulting PTMA brushes/silica nanoparticles with a size of 15, 40, and 400 nm, respectively, have a melted-like morphology. Furthermore, TEM was used to observe the structure of the PTMA brushes/silica nanoparticles. Fig. 1g–i shows TEM images for the PTMA brushes/silica nanoparticles with a particle size of 15, 40, and 400 nm, respectively. When comparing the SEM results, each nodule of 15 and 40 nm-samples is actually composed of several PTMA brushes/silica nanoparticles. However, each nodule of the 400 nm-sample is composed of a single silica sphere because the length of the PTMA brush is not long enough to fully fuse the silica spheres together. The SEM and TEM results indicate that the PTMA brushes fuse together and cover the silica nanoparticles. Thus, the PTMA brushes/silica nanoparticles can serve as binder-free cathode-active materials.

The functional groups of the samples were confirmed by FTIR spectra. Fig. 2a–d shows the FTIR spectra for the silica nanoparticles, initiator modified silica nanoparticles, PTMPM brush/silica nanoparticles, and PTMA brush/silica nanoparticles, respectively. The IR spectrum (Fig. 2a) for the bare silica nanoparticles shows an absorption band at 3476 cm^{-1} which corresponds to the stretching vibrations of hydroxyl groups such as absorbed water and SiO–H [11]. The bands at 1638 and 1111 cm^{-1} correspond to the H–O–H bending of absorbed water and the Si–O–Si asymmetric stretching, respectively. The IR spectrum (Fig. 2b) for the initiator-attached silica nanoparticles displays a weak band at 1721 cm^{-1} which is assigned to a C=O stretching of the ester of the surface initiator as shown in the inset of Fig. 2. The IR spectrum (Fig. 2c) of the PTMPM brush/silica nanoparticles indicates a C–H stretching at 2975 cm^{-1} and a C=O stretching at 1730 cm^{-1} [11]. The IR spectrum (Fig. 2d) of the PTMA brush is very similar to that of the PTMPM brush because the N-O· stretching is relatively weak [12]. Furthermore, the chemical characterization and conversion for TEMPO of the PTMA brushes were measured by ESR. The *g*-factor of the PTMA brush/silica nanoparticles was showed as being 2.0067, which corresponds to a typical NO radical of TEMPO [6]. The conversion of TEMPO is 96.2% after the oxidation. Both the results of FTIR and ESR indicate that the PTMPM brush was successfully grafted on the silica nanoparticles, and was further oxidized to form PTMA brush.

The thermal stability and percentage of PTMA brushes were measured by TGA under an atmosphere of air, as shown Fig. 3. Fig. 3a–c illustrates the TGA of the PTMA brushes/silica nanoparticles with a size of 400, 40, and 15 nm, respectively. All the curves show two major steps of decomposition. The first step of decomposition at 150–300 °C may be assigned to the cleavage of the side

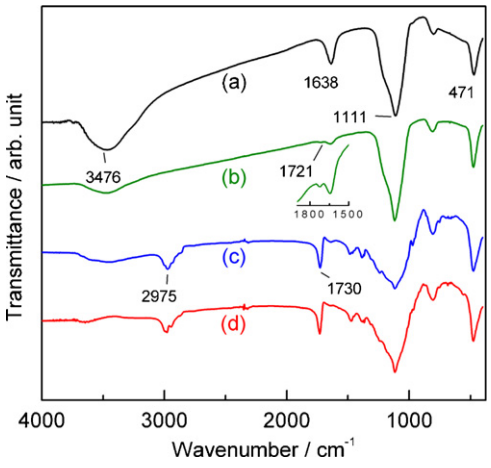

Fig. 2. Infrared spectra for (a) the bare silica nanoparticles (40 nm), (b) the initiator-attached silica nanoparticles, (c) the PTMPM brush/silica nanoparticles, and (d) the PTMA brush/silica nanoparticles. Inset shows zoomed curve (b).

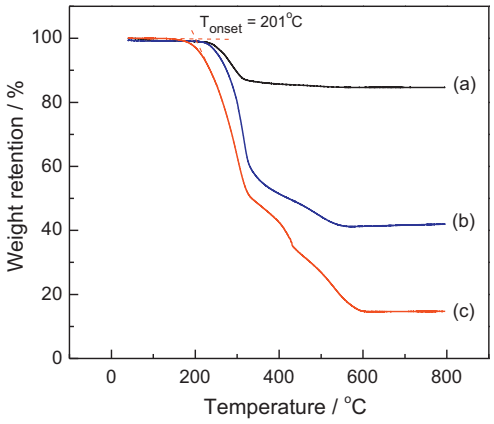

Fig. 3. Thermogravimetric analysis of the PTMA brush/silica nanoparticles with a size of (a) 400, (b) 40, and (c) 15 nm.

chain, TEMPO; the second step at 300–600 °C of decomposition is assigned to the oxidation of the main chain. The decomposition of the onset temperature of the 15 nm-sample was found to be ca. 201 °C. Therefore, the PTMA brushes have a promising thermal stability for the preparation of conventional electrodes. The results also show that the mass retention at 800 °C for the PTMA brushes/silica nanoparticles with a size of 400, 40, and 15 nm is 84.7, 42.0, and 14.7%, respectively. This indicates that the weight loss of the PTMA brushes/silica nanoparticles for 400, 40, and 15 nm silica nanoparticles is 15.3, 58.0, and 85.3%, respectively. When the polymerization time of the brush/silica nanoparticles (15 nm) was increased to 3 h, the weight loss is 90.5%. In the above case, the weight percentage of inactive silica in the electrode is less than 2.5%, which is less than that of the conventional binder addition (~10%). The grafting density of the PTMA brushes on the silica nanoparticles was determined by TGA and GPC using Eq. (1) [13]:

$$\text{grafting density (chains/nm}^2) = \frac{\frac{W_{polymer\ brush}}{100-W_{polymer\ brush}} \times 100 - W_{silica}}{M \times S \times 100} \times N_A \times 10^{-18} \quad (1)$$

where $W_{polymer\ brush}$ and W_{silica} is the weight loss, in percentage, of the polymer brush and silica nanoparticles between 40 and 800 °C. M is the number average molecular weight (M_n = 20,385) of the polymer brush from a free polymer determined by GPC. S is the specific surface area in $m^2\ g^{-1}$ of the silica nanoparticle before grafting. N_A is Avogadro's number, 6.022×10^{23}. The specific surface area of silica nanoparticles, weight loss of the PTMA brushes/silica nanoparticles, weight loss of the nanoparticles, and grafting density of PTMA are summarized in Table 1. The grafting density of the PTMA brushes grafted onto silica nanoparticles with a size of 400, 40, and 15 nm is found to be 0.74, 0.82, and 1.01 chains nm^{-2}, respectively. The grafting density of PTMA brushes grafted on silica nanoparticles is higher than that on ITO, which is 0.24 chains nm^{-2} [9]. These results show that the grafting density of the polymer brushes on silica is denser, and this may be due to a higher reactivity between silica and silanes resulting in a higher density of the surface initiator on silica.

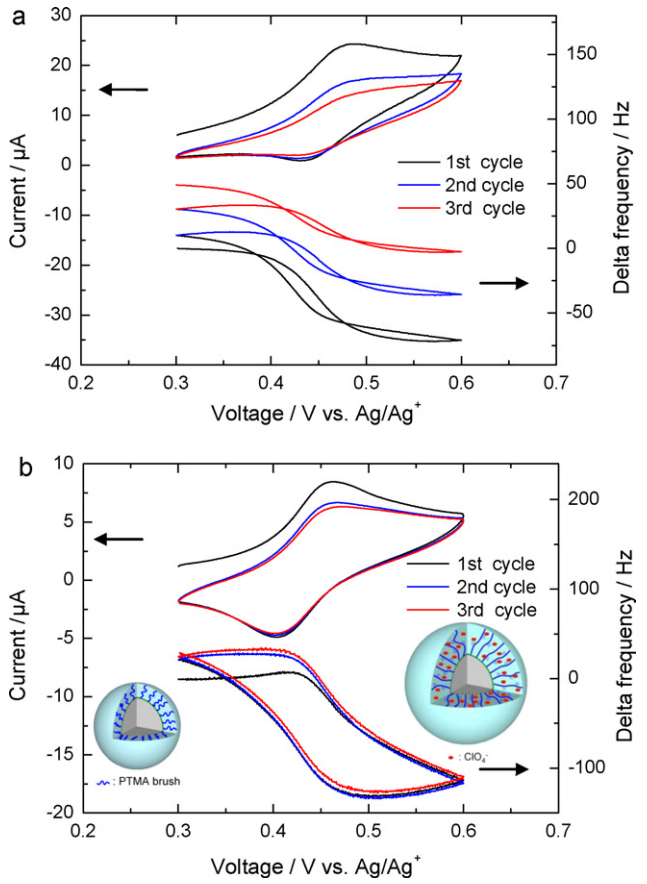

Fig. 4. (a) Cyclic voltammogram (top) for a spin-coated PTMA film on the Au electrode and its corresponding resonance frequency change of EQCM sensor (bottom); (b) cyclic voltammogram (top) for the PTMA brush/silica nanoparticles (400 nm) on the Au electrode and its corresponding resonance frequency change of EQCM sensor (bottom). The electrolyte was 0.1 M $(C_4H_9)_4NClO_4$ in acetonitrile.

Fig. 4a displays the EQCM result for a spin-coated PTMA film on the Au electrode as a control sample. The PTMA was synthesized by ATRP using a free initiator. M_n of PTMA is 11,817. The CV (Fig. 4a) displays an asymmetric redox couple, and its corresponding QCM result indicates that when the nitroxide radicals are oxidized to oxoammonium salts, which gain counterions, the frequency of the QCM decreases. However, as oxoammonium salts are reduced back to neutral nitroxide radicals, the frequency is higher than that in the previous cycle, which may be due to the fact that the oxidation state of PTMA is more hydrophilic and thus the polymer is easily dissolved into polar electrolytes. On the other hand, when the PTMA brushes/silica nanoparticles were deposited on the Au electrode, the CV in Fig. 4b shows a redox couple at about 0.4–0.5 V vs. Ag/Ag^+, which represents a typical PTMA [3]; its corresponding QCM curve is reversible. When the polymer brush is oxidized, the nitroxide radicals gain counterions to form oxoammonium salts as shown in the inset of Fig. 4b. Therefore, the frequency of the QCM decreases. As the oxoammonium salts are reduced

Table 1
Grafting density of PTMA brush/silica nanoparticles.

PTMA brush/silica nanoparticles (nm)	Specific surface area ($m^2\ g^{-1}$)	$W_{polymer\ brush}$ (%)	W_{silica} (%)	Grafting density (chains nm^{-2})
400	6.8[a]	15.3	1.0	0.74
40	50	58.0	0.0	0.82
15	170	85.3	0.3	1.01

[a] This value is estimated by the size of the silica sphere.

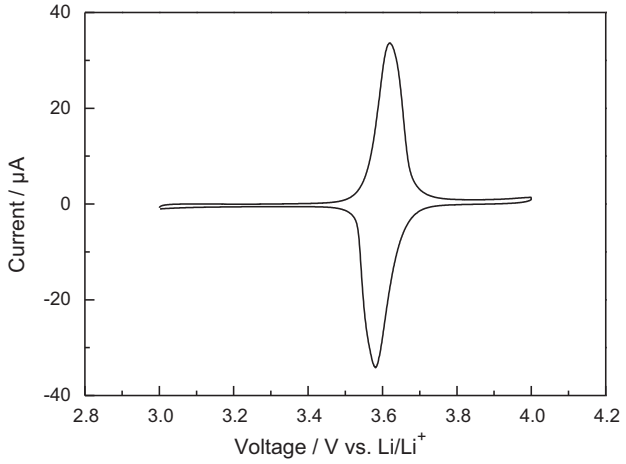

Fig. 5. Cyclic voltammogram for the PTMA brush/silica nanoparticles (40 nm) composite electrode in 1.0 M $LiClO_4$–EC/DEC (=1:1, v/v) at a scan rate of 0.1 mV s^{-1} at 25 °C.

back to the nitroxide radicals, the counterions are removed. Therefore, the frequency reverts to the original frequency. The CV and EQCM curves of the PTMA brush are almost overlapping, which indicate that the PTMA brushes prevent polymers from dissolving into solvents.

Fig. 5 shows a CV of the carbon composite electrode of the PTMA brushes/silica nanoparticles (40 nm) with a redox couple at about 3.6 V vs. Li/Li^+, which is in good agreement with a typical PTMA [2,3,5]. Fig. 6 shows the discharge curves of the PTMA brushes/silica nanoparticles (40 nm) composite electrode at 10, 30, and 50 C. At 10 C, the discharge capacity of the nitroxide polymer brushes electrode is 94.3 mAh g^{-1}. At 30 and 50 C, the polymer brushes electrodes have discharge capacities of 78.6 and 69.2 mAh g^{-1}, respectively. Fig. 7a–c shows the discharge capacities of the PTMA brushes/silica nanoparticles with sizes of 400, 40, and 15 nm, respectively. The results show that the bigger the particle size of silica is, the higher the discharge capacity of the electrode is at various discharge rates. Fig. 8a and b shows the cycle-life performance of the PTMA brush and PTMA composite electrodes at 25 °C, respectively. Fig. 8a shows that the PTMA brush composite electrode has a better cycleability, which is 96.3% retention after 300 cycles [14]. However, Fig. 8b reveals that the discharge capacity of the PTMA composite electrode after 300 cycles is 81.5 mAh g^{-1},

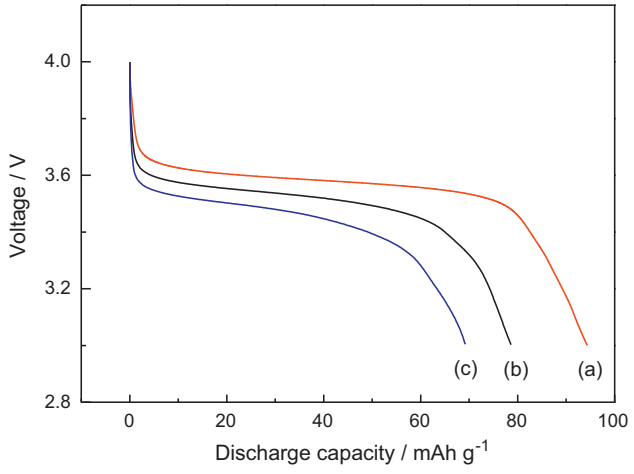

Fig. 6. Discharge curves of the PTMA brush/silica nanoparticles (40 nm) composite cathodes in 1.0 M $LiClO_4$–EC/DEC (=1:1, v/v) at (a) 10, (b) 30, and (c) 50 C at 25 °C.

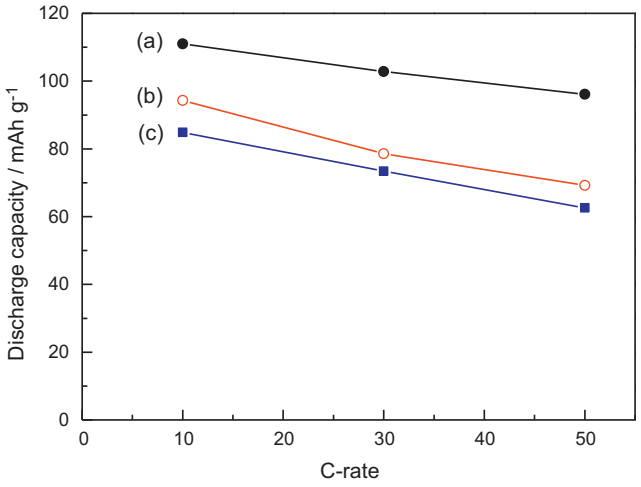

Fig. 7. Discharge capacity of the PTMA brush/silica nanoparticle composite cathodes consisted silica nanoparticles with a particle size of (a) 400, (b) 40, and (c) 15 nm in 1.0 M $LiClO_4$–EC/DEC (=1:1, v/v) at different charge–discharge rates at 25 °C.

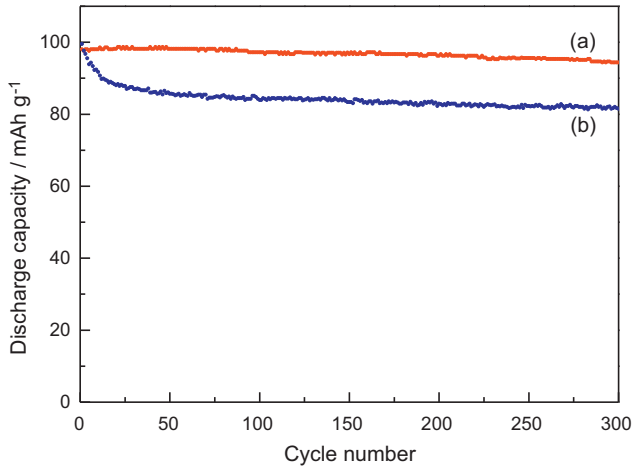

Fig. 8. Discharge capacity as a function of cycle number for (a) PTMA brush/silica nanoparticles (40 nm) and (b) PTMA composite cathodes in 1.0 M $LiClO_4$–EC/DEC (=1:1, v/v) at 10 C rate charge–discharge cycling at 25 °C.

which is 81.9% retention. It is believed that the PTMA electrode displays a significant decrease in capacity in the initial cycles, which may be due to the dissolution of the PTMA in terms of the EQCM results. These results indicate that the PTMA brushes which served as binder-free cathodes are resistant to solvent dissolution. The electrochemical results also show that the PTMA brushes electrodes have a good high rate capacity and cycleability.

4. Conclusions

Non-crosslinking nitroxide polymer brushes grafted onto silica nanoparticles were fabricated by using surface-initiated ATRP to prevent the nitroxide polymer from dissolving into electrolytes and to improve the cycle-life performance of batteries. The non-crosslinking nitroxide polymer brushes/silica nanoparticle electrodes can be processed by slurry coating without the addition of binders. The discharge capacity of the nitroxide polymer brushes is around 84.9–111.1 mAh g^{-1} at 10 C. The PTMA brush composite electrode has a better cycleability, which is 96.3% retention after 300 cycles.

Acknowledgement

The authors are grateful for financial support from the National Science Council of Taiwan.

References

[1] H. Nishide, K. Oyaizu, Science 319 (2008) 737.
[2] K. Nakahara, S. Iwasa, M. Satoh, Y. Morika, J. Iriyama, M. Suguro, E. Hasegawa, Chem. Phys. Lett. 359 (2002) 351.
[3] H. Nishide, S. Iwasa, Y.-J. Pu, T. Suga, K. Nakahara, M. Satoh, Electrochim. Acta 50 (2004) 827.
[4] K. Oyaizu, H. Nishide, Adv. Mater. 21 (2009) 2339.
[5] L. Bugnon, C.J.H. Morton, P. Novak, J. Vetter, P. Nesvadba, Chem. Mater. 19 (2007) 2910.
[6] K. Oyaizu, Y. Ando, H. Konishi, H. Nishide, J. Am. Chem. Soc. 130 (2008) 14459.
[7] T. Suga, H. Konishi, H. Nishide, Chem. Commun. (2007) 1730.
[8] T. Ibe, R.B. Frings, A. Lachowicz, S. Kyo, H. Nishide, Chem. Commun. 46 (2010) 3475.
[9] Y.H. Wang, M.K. Hung, C.H. Lin, H.C. Lin, J.T. Lee, Chem. Commun. 47 (2011) 1249.
[10] W. Stöber, A. Fink, E. Bohn, J. Colloid Interface Sci. 26 (1968) 62.
[11] G. Socrates, Infrared Characteristic Group Frequencies Tables and Charts, 2nd ed., John Wiley & Sons, New York, 1994.
[12] L. Rintoul, A.S. Micallef, D.A. Reid, S.E. Bottle, Spectrochim. Acta Part A 63 (2006) 398.
[13] C. Bartholome, E. Beyou, E. Bourgeat-Lami, P. Chaumont, N. Zydowicz, Macromolecules 36 (2003) 7946.
[14] K. Nakahara, J. Iriyama, S. Iwasa, M. Suguuro, M. Satoh, E. Cairns, J. Power Sources 165 (2007) 398.